HHS Public Access

Author manuscript

J Am Chem Soc. Author manuscript; available in PMC 2021 September 23.

Published in final edited form as:

J Am Chem Soc. 2020 September 23; 142(38): 16334–16345. doi:10.1021/jacs.0c06590.

An interprotein Co-S coordination complex in the B_{12}-trafficking pathway

Zhu Li[1], **Romila Mascarenhas**[1], **Umar T. Twahir**[2], **Albert Kallon**[1,†], **Aniruddha Deb**[3], **Madeline Yaw**[1], **James Penner-Hahn**[3,4], **Markos Koutmos**[3,4], **Kurt Warncke**[2], **Ruma Banerjee**[1,*]

[1]Department of Biological Chemistry, University of Michigan Medical Center, Ann Arbor, MI 48109-0600;

[2]Department of Physics, Emory University, Atlanta, GA 30322-2430;

[3]Department of Chemistry, University of Michigan, Ann Arbor, MI 48109.

[4]Department of Biophysics, University of Michigan, Ann Arbor, MI 48109.

Abstract

The CblC and CblD chaperones are involved in early steps in the cobalamin trafficking pathway. Cobalamin derivatives entering the cytoplasm are converted by CblC to a common cob(II)alamin intermediate via glutathione-dependent alkyltransferase or reductive elimination activities. Cob(II)alamin is subsequently converted to one of two biologically active alkylcobalamins by downstream chaperones. The function of CblD has been elusive although it is known to form a complex with CblC under certain conditions. Here, we report that CblD provides a sulfur ligand to cob(II)alamin bound to CblC, forming an interprotein coordination complex that rapidly oxidizes to thiolato-cob(III)alamin. Cysteine scanning mutagenesis and EPR spectroscopy identified Cys-261 on CblD as the sulfur donor. The unusual interprotein Co-S bond was characterized by X-ray absorption spectroscopy and visualized in the crystal structure of the human CblD thiolato-cob(III)alamin complex. Our study provides insights into how cobalamin coordination chemistry could be utilized for cofactor translocation in the trafficking pathway.

Graphical Abstract

[*]**Corresponding Author**: Ruma Banerjee, 4220C MSRB III, 1150 W. Medical Center Dr., University of Michigan Medical Center, Ann Arbor, MI 48109-0600, Tel: (734) 615-5238; rbanerje@umich.edu.
[†]Albert Kallon, Novartis Pharmaceuticals Corporation, 220 E Hanover avenue, Morris Plains NJ 07950

Supporting Information. Supplementary Figures and Tables. This material is available free of charge via the Internet at http://pubs.acs.org.

The structure factors and coordinates for CblD-thiolato-cob(III)alamin (PDB ID:6X8Z) have been deposited in the Protein Data Bank.

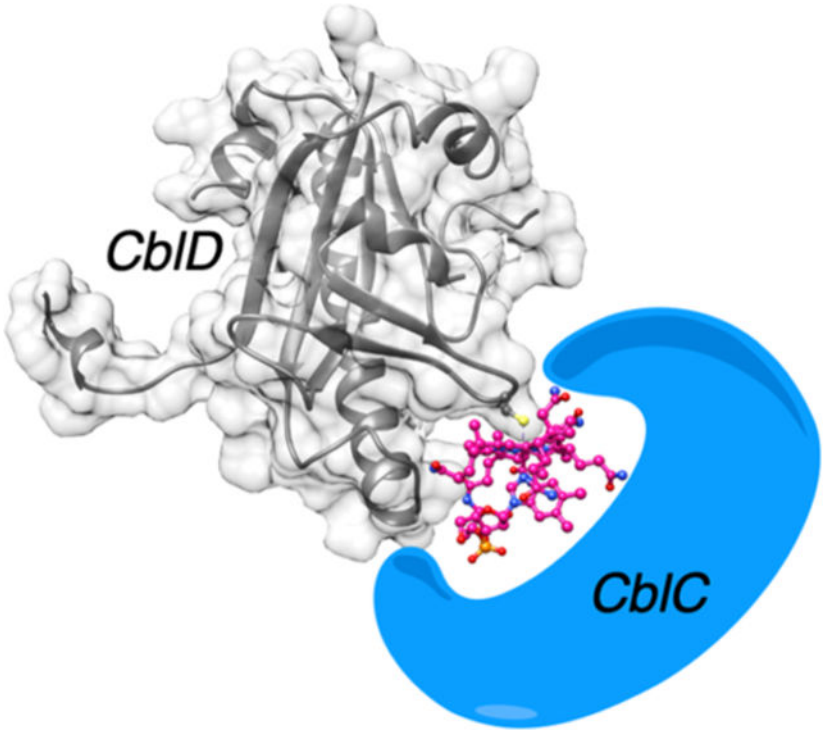

INTRODUCTION

Cobalamin, or the B_{12} cofactor, is required by two mammalian enzymes that are involved in either one-carbon or anaplerotic metabolism. The two biologically active cofactor derivatives, methylcobalamin (MeCbl) and 5'-deoxyadenosylcobalamin (AdoCbl), support methionine synthase and methylmalonyl-CoA mutase, respectively[1]. Chaperoned delivery of B_{12} via an intricate trafficking pathway averts unwanted side reactions and ensures specificity of delivery to its two client proteins[2–4]. Inherited defects in the B_{12} trafficking pathway lead to combined or isolated homocystinuria and methylmalonic aciduria, depending on whether the affected locus is in the common or one of the branched segments in the trafficking pathway[5] .

The *cblC* locus is a mutation hotspot and the most common cause of inborn errors of cobalamin metabolism[6]. It encodes a versatile processing chaperone CblC (or MMACHC) that is characterized by broad substrate and reaction specificity. Thus, CblC removes the upper axial ligand via glutathione (GSH)-dependent dealkylation of alkyl-cobalamins[7] or reductive elimination of cyano-(CNCbl)[8] or aquo-cobalamin (H_2OCbl)[9] (Figure 1a). The resulting cob(II)alamin product formed under aerobic conditions, is subsequently partitioned between the cyto-plasmic and mitochondrial branches of the B_{12} trafficking pathway, to support methionine synthase and methylmalonyl-CoA mutase function, respectively.

While CblC has been characterized extensively,[7–18] much less is known about the role of CblD (or MMADHC) in the trafficking pathway. Structures of CblD missing approximately a third of its N-terminal segment that is predicted to be largely disordered, have revealed that

it most closely resembles CblC[19, 20]. Both CblC and CblD belong to the flavin nitroreductase super-family and likely originated via a gene duplication event. CblD can form a complex with CblC, albeit only when cobalamin lacking an upper axial ligand is bound to CblC[21–23]. However, unlike CblC, direct binding of cobalamin to CblD has not been observed[22].

The two axial ligand positions in cobalamin provide potential coordination handles for its movement between proteins. The internal dimethylbenzimidazole (DMB) base, which is appended from the corrin ring, occupies the lower axial position in solution but is pried away from the cobalt in all human trafficking proteins that have been characterized so far (Figure 1a). The so-called “base-on” state of cobalamin specifically refers to coordination by a nitrogen ligand in the DMB base. Here, we demonstrate that cobalt-sulfur (Co-S) coordination is a molecular feature of the protein-protein complex between CblD and cobalamin bound to CblC. Biophysical and crystallographic analyses revealed that CblD alone can coordinate cobalamin directly, which was likely missed previously due to oxidation of the coordinating Cys-261 residue in the protein, as isolated. The interprotein Co-S coordination complex between CblC and CblD suggests a mechanism for cobalamin translocation and clues into how this large cofactor is moved between active sites in the B_{12} trafficking pathway.

RESULTS

CblC and CblD form a complex via Co-S coordination

Complex formation between CblC and CblD was monitored by UV-visible spectroscopy. Addition of CblD to cob(II)alamin-loaded CblC under aerobic conditions, resulted in a shift of the 473 nm peak to a spectrum with absorption maxima at 427 nm and 499 (with isosbestic points at 441, 493 nm) (Figure 1b, Scheme 1 reaction 1). The new spectrum resembles that reported for base-off thiolato-cob(III)alamin with absorption maxima at 425 and 498 nm[24]. The base-off conformation was expected, based on the crystal structure data of cobalamin bound to CblC[1618]. A 1:1 stoichiometry was observed for complex formation between CblC and CblD (Figure 1c). The k_{obs} for thiolato complex formation (4 ± 1 min^{-1}) was obtained from the fast phase of the reaction in which the major amplitude change was observed (Figure 1d).

Formation of the CblD-CblC complex was also observed during dealkylation of MeCbl by CblC under aerobic conditions (Figure 1e, *upper*). Thus, addition of GSH to MeCbl-loaded CblC (457 nm) in the presence of CblD, promoted dealkylation and formation of the thiolato complex (with isosbestic points at 371, 394, 436 and 488 nm) (Scheme 1 reaction 2). The conversion of cob(I)alamin to thiolato-cob(III)alamin (Scheme 1, reaction 2) proceeds via multiple steps, i.e. initial oxidation of the cob(I)alamin product to cob(II)alamin (*reactions 3–4*), complex formation with Cys-261 in CblD, and oxidation of thiolato-cob(II)alamin to form the CblD-S-thiolato-Cob(III)-CblC complex (*reactions 5-6*). The presence of CblD did not affect the dealkylation kinetics of CblC (0.048 ± 0.004 min^{-1}, Figure S1a); the k_{obs} was ~100- fold slower than for thiolato complex formation between CblD and CblC.

In the absence of CblD, cob(I)alamin formed during the demethylation reaction was oxidized to H_2OCbl (Scheme 1 reaction 7) with maxima at 355 and 523 nm (and isosbestic points at 336, 370 and 486 nm) (Figure1e, *lower*). While cob(II)alamin bound to CblC is resistant to air oxidation[1924], it is oxidized by superoxide to aquo-cob(III)alamin, generated *in situ* during oxidation of cob(I)alamin (*reaction 4*). The redox potential for base-off H_2O-cob(III)alamin/cob(II)alamin is +510 mV, which is 310 mV more positive than for the base-on species[25]. The difference in redox potentials for the $O_2/O_2^{\bullet-}$ (−330 mV) and $H_2O_2/O_2^{\bullet-}$ (+940 mV)[26] couples explains the susceptibility of CblC-bound cob(II)alamin to oxidation by superoxide but not by oxygen.

The N- and C-termini of CblD and CblC, respectively, are predicted to be largely disordered and are not required for complex formation, as previously demonstrated[2022]. Consistent with these data, formation of the thiolato complex was also observed with the truncated variants of $CblC^{\Delta C}$ and $^{\Delta N}$CblD missing 38 and 116 residues respectively (Figure S1b). Using size exclusion chromatography, we characterized complex formation using the truncated variants, which are more stable (Figure 1f). Complex formation was observed in the presence of cob(II)alamin but not in its absence. The complex also did not form in the presence of MeCbl, highlighting the importance of cob(II)alamin for forming a stable interprotein complex.

Cys-261 in CblD provides the thiolato ligand to cobalamin

We reasoned that the thiolato ligand in the CblD•CblC complex is donated by a cysteine residue in one of the two proteins. Since iodoacetamide alkylation of $^{\Delta N}$CblD precluded complex formation (Figure S2a), we used cysteine scanning mutagenesis to identify the ligand donor. Mutation of Cys-148, Cys-153, Cys-212 or Cys-262 did not noticeably affect complex formation, whereas mutation of Cys-261 to serine or methionine diminished it by ~75% and 90% respectively (Figure S2b,c). The residual complex seen with the C261S/M mutants could be due to partial substitution by the vicinal Cys-262 residue, which was abolished in the C261S/C262S double mutant. Thiolato-cobalamin formation was, however, not observed by UV-visible spectroscopy upon mixing C261S CblD with cob(II)alamin bound to CblC, indicating that if present, its concentration is low (Figure 1g). Notably, Cys-261 and Cys-262 are conserved in CblD from worm to man. Together, our results identified Cys-261 as the sulfur ligand donor to cobalamin and illustrated its importance in forming a stable CblD•CblC complex.

Molecular basis of the CblD•CblC coordination complex

Next, we aimed to understand the chemical mechanism by which the coordination complex forms between CblD and CblC. Specifically, we asked whether ligand exchange requires cob(III)alamin or cob(II)alamin or can occur at either oxidation state. To distinguish between these mechanisms, CblC•H_2OCbl was first generated via dealkylation of MeCbl (Figure 1e, *lower*). Following removal of excess GSH and addition of CblD, thiolato-cob(III)alamin formation was not seen even after 1 h (Figure S3a), which is in sharp contrast to its rapid formation when MeCbl was dealkylated *in situ* in the presence of CblD (Figure 1e, *upper*). This observation is consistent with ligand exchange in base-off cob(III)alamin being disfavored[27]. In contrast, and as discussed in greater detail below, exchange of the

water ligand in base-off cob(II)alamin by the thiolate of Cys-261 in CblD led to complex formation.

Next. we further probed the mechanism by which complex formation occurs by assessing whether a paramagnetic thiolato-cob(II)alamin intermediate was formed (Scheme 1 reaction 5). To stabilize this intermediate against oxidation, EPR experiments were conducted under anaerobic conditions. The EPR spectrum of CblC$^{\Delta C}$•cob(II)alamin is typical of a 5-coordinate base-off species in which DMB is replaced by a water ligand (Figure 2a). It is characterized by a broad spectrum with rhombic *g*-anisotropy that features a signature low-field peak (261 mT) associated with the g_x value, and by Co (I=7/2) hyperfine octet splitting of narrow troughs, centered at the g_z value. The lines appear as singlets rather than triplets indicating that the cobalt is coordinated to water rather than to nitrogen (I=1). Addition of $^{\Delta N}$CblD led to dramatic changes in the EPR spectrum (Figure 2b), which was distinguished by the appearance of a second line shape with a contracted set of high-field trough features distributed about a comparable g_z position, and a peak feature near 290 mT. Deconvolution of this spectrum by subtraction of the scaled spectrum of the CblC•cob(II)alamin revealed that the new features arise from a species with axial *g*-tensor symmetry (Figure 2c) that represents ~36% of the composite signal. The line shape is well-matched by the spectrum of the model glutathionyl-cob(II)inamide compound, where GS^- serves as the axial thiolato ligand (Figure 2d). Based on this comparison, the new species seen in the presence of CblD was assigned to thiolato-cob(II)alamin in the CblD•CblC complex. EPR simulations further supported and quantified the assignment (Figure S4a,b, Table S1). When C261S $^{\Delta N}$CblD was used instead of the wild-type protein, the thiolato-cob(II)alamin signal was significantly diminished (Figure 2e), supporting the assignment of Cys-261 as the primary ligand donor in the CblD•CblC complex. The EPR data thus support a mechanism in which interprotein Co-S ligation occurs at the cob(II)alamin oxidation state.

When $^{\Delta N}$CblD was added to free cob(II)alamin, which prefers 5-coordinate geometry, the spectrum revealed the presence of Co-N coordination as signaled by the triplet superhyperfine splittings, indicating that the Cys-261 did not exchange with the DMB ligand (Figure 2f). In contrast, addition of $^{\Delta N}$CblD cob(II)inamide revealed a mixed spectrum (Figure 2g) with contributions from: (i) H_2O-cob(II)inamide, (ii) thiolato-cob(II)inamide, and (iii) a cob(II)inamide species characterized by a *g*-tensor rhombicity intermediate between the O-liganded H_2O-cob(II)alamin and the axial spectra of the N- and S-liganded species (Figure 2h). The absence of superhyperfine splitting of the ^{59}Co hyperfine octet around g_z (indicating an axial ligand with I=0) and the dominant dependence of *g*-tensor rhombicity on the strength of the axial Co-ligand bond (i.e. relative insensitivity to corrin ring conformation; weak aquo ligand ruled-out)[28] leads to assignment of the spectrum in Figure 2h to a cob(II)inamide-$^{\Delta N}$CblD interaction characterized by a relatively long Co-S bond, associated with a degree of corrin ring distortion that is intermediate between free cobinamide (aquo ligand) and one with a sterically bulkier axial thiolato-(either CblD-cysteinyl or glutathionyl-) ligand.

The ability of $^{\Delta N}$CblD to form a thiolato- complex with cob(II)inamide, but not with cob(II)alamin is surprising for at least two reasons. It reveals, for the first time, the ability of CblD to independently bind cobalamin and shows that while Cys-261 undergoes ligand

exchange with the relatively weak axial H_2O ligand, it is unable to displace the stronger, internal DMB ligand in cob(II)alamin. These data illuminate the critical importance of binding cob(II)alamin in the base-off form in CblC$^{\Delta C}$, further supporting the sequence of CblD•CblC formation in which the interprotein coordination is established at the cob(II)alamin oxidation state (Scheme 1 reaction 5), prior to a one-electron oxidation to thiolato-cob(III)alamin (Scheme 1 reaction 6).

To further test this mechanism, $^{\Delta N}$CblD was mixed with CblC$^{\Delta C}$•cob(II)alamin under anaerobic conditions (Figure S3b), which elicited only minor changes in the cob(II)alamin absorption spectrum. This was expected since replacement of the aquo with a thiolato ligand in the model cob(II)inamide compound similarly elicits only minor spectral changes (Figure S4c). Introduction of air led to significant spectral changes, signaling formation of thiolato-cob(III)alamin (Figure S3b). Thus, while water-ligated cob(II)alamin bound to CblC$^{\Delta C}$ is air-stable (Figure 1b)[19], which is a characteristic of base-off cob(II)alamin[25], it is susceptible to ligand exchange in the CblD•CblC complex consistent with a change in the ligand environment. Notably, under anaerobic conditions, which precluded further oxidation, the yield (~36%) of the thiolato-cob(II)alamin complex was low (Figure 2b, Scheme 1 reaction 5). In contrast, under aerobic conditions, which allowed subsequent oxidation to thiolato-cob(III)alamin, complex formation was stoichiometric with the amount of CblC-bound cobalamin (Figure 1b, Scheme 1 reaction 6). Together, our data indicate that thiolato-cob(III)alamin formed via oxidation of the initial thiolato-cob(II)alamin species, drives stabilization of the CblD•CblC complex.

CblD binds H_2OCbl and forms a complex with CblC

Coordination of cob(II)inamide by CblD (Figure 2g) was surprising as previous studies had concluded that CblD does not bind the cofactor directly[2022]. It also raised the possibility of a model in which the cofactor can initially bind to either protein prior to formation of the CblD•CblC complex. To assess this alternative model, we characterized the binding of H_2OCbl (λ_{max}= 351, 526 nm) to CblD, which resulted in spectral changes consistent with the formation of base-on thiolato-cob(III)alamin[2429] (λ_{max}= 334, 372, 531 nm) (Figure 3a) and yielded K_D values of 1.0 ± 0.4 μM (wild-type CblD) and 9.1 ± 1.6 μM ($^{\Delta N}$CblD) (Figure S5a). The k_{obs} for the ligand exchange (Scheme 1 reaction 9) was 0.085 ± 0.004 min^{-1}, which was 50-fold lower than for the formation of thiolato-cob(III)alamin via the interaction of CblD with CblC•cob(II)alamin (Figure 1d). Either Cys-261 or Cys-262 in CblD could coordinate free H_2OCbl as evidenced by thiolato-cob(III)alamin formation with either single mutant but not with the double mutant (Figure 3a *inset*).

The resistance of the CblC•H_2OCbl complex to ligand exchange by Cys-261 on CblD (*reaction 8*, Figure S3a) versus free H_2OCbl (*reaction 9*, Figure 3a), is explained by the difference in their coordination environments. While CblC-bound H_2OCbl is base-off, free H_2OCbl is base-on, facilitating a dissociative ligand exchange reaction[27]. Similarly the ability of CblD to coordinate H_2OCbl but not cob(II)alamin is influenced by the difference in the preferred coordination numbers for Co^{2+} (5) versus Co^{3+} (6). Thus, while a thiolato group on CblD can replace the water-ligand in free H_2OCbl, (Scheme 1 reaction 9, Figure 3a), it cannot replace the Co-N ligand in cob(II)alamin (Figure 2f), illustrating how the

cobalt redox state controls coordination chemistry and in turn, susceptibility to ligand exchange.

Next, we assessed whether the CblD•CblC complex can form when cob(III) alamin is coordinated to CblD. Mixing C262S $^{\Delta N}$CblD-thiolato-cob(III)alamin with CblC$^{\Delta C}$ resulted in complex formation (Figure 3b). The spectral changes were consistent with the conversion of the base-on CblD-thiolato-cob(III)alamin to the base-off form in the CblD•CblC complex. The resulting absorption spectrum and elution profile (Figure S5b) of the complex were very similar to that of the complex formed when CblC was the cobalamin carrier. The K_D for complex formation was estimated to be 40 ± 20 nM by isothermal titration calorimetry (Figure S5c), indicating a 200-fold higher affinity for the interprotein complex than between C262S $^{\Delta N}$CblD and H_2OCbl. The efficiency of complex formation was significantly lower with the C261S variant even in the presence of a 5-fold excess of CblC$^{\Delta C}$ (Figure S6). We speculate that coordination to Cys-262 rather than the preferred Cys-261 ligand sterically hinders complex formation.

Characterization of the Co-S bond by XAS

Since Co-S ligation is rare in nature, we further characterized the thiolato-cob(III)alamin complex by XAS. The XANES spectrum of the thiolato-cob(III)alamin complex of $^{\Delta N}$CblD was compared to that of the model GSCbl compound, both in the base-on state (Figure 3c). These two spectra are nearly identical, as are the XANES spectra for the $^{\Delta N}$CblD•CblC$^{\Delta C}$ (± GSMe). While all four complexes have similar spectra, it is clear that they fall into two groups: the base-on $^{\Delta N}$CblD-thiolato-cob(III)alamin and GSCbl have higher intensity and better resolved shoulders at 7725 eV compared to the base-off $^{\Delta N}$CblD•CblC$^{\Delta C}$ complexes. The energy of the edge at half-maximum correlates with cobalt oxidation state[30]. The observed energies are: 7720.0 eV ($^{\Delta N}$CblD-thiolato-cob(III)alamin) and 7720.6 eV (GSCbl) for the base-on samples and are nearly identical for the base-off thiolato-cob(III)alamin in the $^{\Delta N}$CblD•CblC$^{\Delta C}$ complex (7720.0 (+GSMe) and 7720.2 eV (−GSMe)). These values are comparable to those reported for authentic cob(III)alamin[30], and significantly higher than for cob(II)alamins (~7718 eV), and did not change during data collection, indicating that the sample remained in the Co^{3+} oxidation state. In all cases, the weak 1s→3d pre-edge transition was consistent with the presence of an approximately centrosymmetric cobalt ion.

The k^3 weighted EXAFS and Fourier transform data for all four samples are, to a first approximation, quite similar (Figure S7,8). A careful comparison however, revealed that the amplitude at k ~6.7 Å^{-1} is higher and that at k ~8 Å^{-1} is lower for the base-off versus the base-on samples. Similarly, the position of the second peak in the Fourier transform (R+α ~2.3 Å) is slightly shorter for the base-on than the base-off samples, suggesting that the variability at k ~6–8 Å^{-1} might be arising from interference from scatterers outside the Co-N shell (Figure 3d).

The EXAFS data for the base-on thiolato-cobalamins were best fit in the cobalt nearest neighbor environment with 5 Co-N/O bonds at 1.89 Å and a single Co-S bond at a distance of 2.23–2.24 Å (Table S2). The data for the base-off thiolato-cob(III)alamin samples were best fit with the same Co-N /O distance but did not show evidence for a short (~2.2–2.3 Å) Co-S shell. Fits to these spectra were improved slightly if a longer, 2.56–2.57 Å, Co-S shell

was included. We note however, that it is difficult from EXAFS data alone to define such a long Co-S interaction.

Crystal structure of the $^{\Delta N}$CblD-thiolato-cob(III)alamin complex

To gain structural insight into how cobalamin binds to CblD, we used the C262S $^{\Delta N}$CblD variant, which stabilizes the thiolato complex (Figure S2c). The crystal structure of the $^{\Delta N}$CblD-thiolato-cob(III)alamin complex was obtained at 2.5 Å by molecular replacement (Table S3). Difference electron density for cobalamin was seen in both chains in the asymmetric unit and could be modeled as the base-on species in one chain (occupancy=1.0) (Figure 4a), while density for the DMB nucleotide moiety was missing in the second (occupancy=0.9). Surprisingly, virtually no interactions were observed between the corrin ring and $^{\Delta N}$CblD with the exception of a hydrogen bond between an acetamide side chain of pyrrole ring c and the backbone amide of Thr-187 (Figure 4b). At the upper axial position, continuous electron density between Cys-261 and the cobalt atom was seen and the Co-S bond was constrained based on the EXAFS data to 2.2 Å. Coordination to cobalamin did not induce a significant conformational change in the Cα backbone of $^{\Delta N}$CblD, which was superimposed on the structure of the truncated apo-protein with an RMSD of 0.63 Å (Figure S9).

DISCUSSION

Elaborate systems for the sequestration and chaperoned delivery of metal cofactors have evolved to ensure specificity of metal reconstitution and to suppress spurious solution reactivity. A common strategy seen in metal trafficking pathways is that cargo is transferred in associative protein-protein complexes that are formed transiently only when the donor protein is loaded with the cofactor[31]. The redox state, coupled to the preferred metal coordination geometry, are critically important for metal migration in trafficking pathways, while a gradient of increasing affinities provides the thermodynamic driving force. Interchanging sulfur (e.g. cysteine or GSH) and nitrogen (e.g. histidine) coordination is commonly used for metal translocation. In this context, while Co-N coordination is common, Co-S coordination is very rare in nature.

Compared to other metal cofactors, cobalamin trafficking poses the additional logistical challenge of moving cargo with a molecular mass of at least 1328 Da. By comparison, the structurally similar heme cofactor is less than half the size (614 Da) although very little is also known about its intracellular trafficking[32]. Depending on the oxidation state and whether or not DMB serves as a ligand, cobalamin can present 1 to 2 vacant coordination sites in the Co^{2+} and Co^{3+} oxidation states. In the base-off state, the extended DMB tail potentially provides an additional “handle” to control cofactor movement between active sites.

Prior to this study, it was known that CblD can form a cobalamin-dependent complex with CblC but was believed to lack the capacity to bind the cofactor independently[2022]. Indeed, the crystal structure of human apo-CblD appeared to support this conclusion. It revealed that despite molecular mimicry of CblC, the region corresponding to the large cobalamin binding pocket in CblC is largely occluded by amino acid side chains in CblD[19]. Our discovery of

Co-S mediated interprotein coordination in the CblD•CblC complex, and the ability of CblD to coordinate cobalamin directly, was therefore unexpected. It raised a number of questions including why the thiolato-cobalamin complex with CblD was missed previously, while CblD•CblC complex formation, albeit inefficient[22], was seen. We speculate that cysteine oxidation during CblD purification led to its inability to bind H_2OCbl via ligand exchange, which is supported by our observation that reduction followed by removal of excess DTT is needed to observe stoichiometric cobalamin binding. During formation of the CblD•CblC complex on the other hand, excess GSH was added to catalyze the dealkylation or decyanation of MeCbl or CNCbl to generate cob(II)alamin *in situ*[22], which presumably led to reduction of the cysteine residues on CblD.

Very few examples of naturally occurring Co-S coordination systems have been described so far, and none involves an interprotein coordination complex. Co-S coordination is postulated in the mercury methyltransferase HgcA[33], and has been visualized in the cobalamin transporter BtuM[34]. The structure of the thiolato-cob(III)alamin complex with CblD revealed a Co-S bond, with a 2.24 Å bond length as inferred from the EXAFS data. In both CblD and BtuM, the cobalt ion is axially coordinated by thiolato- and nitrogen ligands, although their orientation is reversed. DMB is replaced by a cysteine ligand on the α-face in BtuM while the β-axial ligand position is occupied by a histidine residue. The slow kinetics and the relatively high K_D for H_2OCbl binding to CblD, suggest that direct interaction between CblD and H_2OCbl is unlikely to be physiologically relevant.

A common theme in metal trafficking pathways is that the cofactor binding site in protein chaperones is often solvent exposed, enabling access of a ligand in the acceptor protein for coordination to the metal in the donor protein, setting up the transfer process[31]. This is also the case with CblC where the cobalamin resides in a solvent accessible binding pocket and the DMB tail extends into a shallow, surface exposed groove (Figure 5a). While the structure of the CblD•CblC complex has eluded us so far, we note a number of features in the individual proteins that might be relevant to its formation and to downstream interactions. A ring of arginine residues (Arg-111, Arg-144 and Arg-201) frames the active site of CblC, forming a highly electropositive entrance (Figure 5b). We posit that the Cys-261 carrying β-hairpin loop in CblD accesses the cobalt ion from the β-face, which faces a commodious cavity. A patch-work of charges is seen on the β-hairpin loop with electronegative Asp-257 and Asp-258 and electropositive Lys-263 and Arg-266 on either side of Cys-261 and Cys-262 (Figure 5c). The L259P patient mutation resides on this loop and decreases the rate of CblC•cob(II)alamin oxidation 4-fold[19]. EXAFS data are consistent with a long Co-S bond length (~2.57 Å, although not well defined) in the CblD-thiolato-cob(III)alamin•CblC complex, which is in good agreement with the unusually long 2.7 Å Co-S bond found in BtuM[34]. It is significantly longer than the Co-S distance in GSCbl and in the thiolato-cob(III)alamin complex in CblD (2.2Å), which are base-on (Table S2). We note that a model of the CblD•CblC complex generated from low resolution SAXS data positioned the β-hairpin loop away from the CblC active site and is unlikely to be correct[20].

CblD coordinates to CblC when the cofactor is present in the cob(II)alamin oxidation state (Figure 5d). The resulting thiolato-cob(II)alamin protein complex has, to our knowledge, been characterized for the first time by EPR spectroscopy (Figure 2). Thiolato-

cob(III)alamin formed via oxidation, has been characterized by XAS spectroscopy (Figure 3c,d). Intriguingly, a subset of patient mutations in CblD suppresses the oxidation of CblC-bound cob(II)alamin[19], suggesting a functional role for this reaction in the trafficking pathway. Furthermore, the redox sensitivity of the vicinal cysteines in CblD suggest that they might serve as a possible regulatory switch, which we are currently testing. The cap domain in CblC extends into the C-terminus that is predicted to be disordered as is the N-terminal third of the CblD. While these regions are dispensable for complex formation, they might be important for facilitating downstream interactions of the CblD•CblC complex with partner proteins. The N-terminal third could also be important for organizing a cobalamin binding pocket in CblD, which is missing in the crystal structure reported here. Notably, the nonsense mutations in CblD R250X, S228X[35] lead to truncations upstream of Cys-261, and would be predicted to impair CblD•CblC complex formation if these variants are stably expressed.

In summary, we have identified a previously unseen Co-S dependent protein-protein complex in the human cobalamin trafficking pathway, illuminating the molecular role of CblD as the sulfur ligand donor. Complex formation is exquisitely sensitive to the cobalt oxidation state, which in turn, is linked to the preferred coordination geometry. While either cob(II)alamin bound to CblC or cob(III)alamin bound to CblD can initiate CblD•CblC complex formation, kinetic and thermodynamic considerations strongly favor the former over the latter and provide insights into the sequence of processing and translocation events in cobalamin trafficking.

EXPERIMENTAL SECTION

Materials

Cob(II)alamin was generated by photolysis of AdoCbl anaerobically as described previously[36] . Cob(II)inamide was generated by photolysis of adenosyl-cobinamide, which was synthesized and purified as described[37] . GSH, GSMe, H_2OCbl, AdoCbl, MeCbl and superoxide dismutase (SOD) were purchased from Sigma-Aldrich.

Expression and purification of human CblC

Full-length human CblC was cloned using the ligation-independent cloning (LIC) vector with an N-terminal His_6-tag, using the forward primer TACTTCCAATCCAATGCAATG-GAGCCGAAAGTCGC (forward) and TTATCCACTTCCAA-TGTTATTAAGGGCCAGGGGATGCA (reverse). Due to stability issues with full-length CblC, a previously characterized a more stable C-terminal truncated form (1–244) with a C-terminal His_6-tag[16], which was used in this study and is referred to as $CblC^{\Delta C}$.

Recombinant human CblC was purified from *E. coli* BL21 (DE3) transformed with LIC-CblC or pET28-$CblC^{\Delta C}$ and grown overnight at 37 °C in 100 mL of Luria Bertani (LB) medium containing ampicillin (100 μg•mL^{-1}) or kanamycin (50 μg•mL^{-1}) respectively. Then, 6 × 1 L of LB medium containing the corresponding antibiotics was inoculated with the starter culture and grown at 37 °C. After 4 h, when the OD_{600} had reached 0.5–0.6, the temperature was reduced to 15 °C. The cultures were induced with 100 μM isopropyl β-D-1-

thiogalactopyranoside (IPTG) and the cells were harvested 16 h later. The cells pellets were stored at −80 °C until use.

Cell pellets were suspended in 200 mL of lysis buffer (50 mM Tris-HCl, pH 8.0, 300 mM KCl, 15 mM imidazole) supplemented with 0.15 mg•mL^{-1} lysozyme, and 1 tablet of EDTA-free cOmplete™ Protease Inhibitor Cocktail (Roche). The cell suspension was stirred at 4 °C for 20 min and then sonicated (power setting = 5) on ice for 8 min at 15 s intervals separated by 60 s cooling periods. The sonicate was centrifuged at 38,000 × g for 30 min and the supernatant was loaded onto a Ni-NTA-agarose column (2.5 × 5 cm, Qiagen) pre-equilibrated with the lysis buffer. The column was washed with 100 mL of the lysis buffer + 30 mM imidazole and eluted with 300 mL of a linear gradient ranging from 30 mM to 300 mM imidazole in the lysis buffer. The fractions containing CblC were identified by SDS-PAGE analysis, pooled and concentrated. The resulted proteins were dialyzed into the Reaction Buffer containing 100 mM HEPES-KOH, pH 7.4, 150 mM KCl and 10% glycerol, and the protein monomer was separated from oligomers by size exclusion chromatography (Superdex 200, 100 mL, GE Healthcare) and stored at −80°C. All assays were performed in the Reaction Buffer unless otherwise specified.

Cloning, expression and purification of CblD

Full length human CblD was cloned into the pGEX-4T1 vector using the BamHI/XhoI restriction enzyme sites to generate the N-terminal GST-tagged construct, pGEX-CblD. The sequence of the forward and reverse primers used for cloning were: CGCGTGGATCCATGGCC-AATGTGCTTTGTA and CGGCCGCTCGAGTTAATTTCCACTTAATTTCTTC. Since thrombin exhibits non-specific activity and tended to cleave CblD, we replaced the thrombin cleavage site between GST and CblD by the TEV-protease cleavage site (pGEX-TEV-CblD) using site-directed mutagenesis. The sequences of the primers were: GAGAACCTGTACTTCCAATCCGGATCC-ATGGCCAATGTGCT (forward); GGATTGGAAGTAC-AGGTTCTCATCCGATTTTGGAGGATGGTC (reverse).

E. coli BL21 (DE3) was transformed with pGEX-TEV-CblD and grown overnight at 37 °C in 100 mL of Luria Broth medium containing ampicillin (100 μg•mL^{-1}). Then, 6 × 1 L of LB medium containing ampicillin (100 μg•mL^{-1}) was inoculated with the starter culture and grown at 37 °C. After 4 h, when the OD_{600} had reached 0.5–0.6, the temperature was reduced to 15 °C. The cultures were induced with 200 μM IPTG and the cells were harvested 16 h later. The cells pellets were stored at −80 °C until use. For purification, the cell pellets were suspended in 200 mL of buffer containing 50 mM Tris-HCl, pH 7.4, 50 mM KCl, 20 mM β-mercaptoethanol (β-ME), 0.15 mg•mL^{-1} lysozyme, and 1 tablet of EDTA-free cOmplete™ Protease Inhibitor Cocktail (Roche). The cell suspension was stirred at 4 °C for 20 min and then sonicated (power setting = 5) on ice for 8 min at 15 s intervals separated by 60 s cooling periods. The sonicate was centrifuged at 38,000 × g for 30 min and the supernatant was loaded on a GSH-agarose column (2.5 × 5 cm, GE Healthcare) pre-equilibrated with Buffer A (50 mM Tris-HCl, pH 7.4, 50 mM KCl). The column was washed with 100 mL of Buffer A and eluted with 100 mL of 10 mM GSH in Buffer B (50 mM Tris-HCl, pH 8.0, 50 mM KCl). The fractions containing GST-CblD were identified by SDS-

PAGE analysis, pooled and dialyzed with 1.5 mg TEV-protease overnight against 1 L Buffer A + 10 mM β-ME. The dialyzed protein was loaded on to a second GSH agarose column (2.5 × 5 cm) pre-equilibrated with Buffer A. The column was further washed with 30 mL of Buffer A. CblD lacking the GST tag, eluted in the flow-through and was concentrated to 5 mL and dialyzed against 0.5 L Reaction Buffer + 4 mM dithiothreitol (DTT) overnight at 4 °C. The protein monomer was separated from oligomers by size exclusion chromatography (Superdex 200, 100 mL, GE Healthcare) in the Reaction Buffer and stored at −80°C. In order to ensure all cysteines were reduced, CblD was treated with 20 mM DTT overnight on ice, prior to any experiments. DTT was removed by extensive washing with the Reaction Buffer in an Amicon centrifugation devices (MWCO=10 kDa, Sigma-Aldrich).

Cloning, expression and purification of CblD mutants

Due to stability issues with full-length CblD, an N-terminally truncated form of CblD (116–296) with improved stability is referred to as $^{\Delta N}$CblD. The CblD mutations were introduced into the previously described pET28-His6-$^{\Delta N}$CblD construct[22] using Quikchange kit (Qiagen). The sequences of the forward primers are noted below; the reverse primers had complementary sequences.

C148S: TCTGCAATACAAACATGTCCAGAATTGCTGCGAAAAGAT;

C153S: AATACAAACATCTCCAGAATTGCTGCGAAAA;

C212S: GGAAATTTCCTATGCTCTTCGAGCTGAGG;

C261S: GACCTTGGATCCTGTAAAGTGATTCGTCATAGTCTC;

C261M:TCTGTTGATGACCTTGGAATGTGTAAAGTGATTCGT
CATAGTCTCTGGGGT;

C262S: CCTTGGATGCTCTAAAGTGATTCGTCAT-GTCTCTGG;

C261S/C262S: TCCTCTAAAGTGATTCGTCATAGT-CTCTGG

The expression and purification of His_6-$^{\Delta N}$CblD mutants was carried out as described previously[22] with the following modification. The His_6-tag was removed during overnight dialysis with TEV-protease (CblD$^{\Delta N}$:TEV protease 100:1 w/w) against 1 L of Buffer C (50 mM Tris-HCl, pH 8.0, 150 mM KCl, 5 % glycerol) + 1 mM DTT. The dialyzed protein was loaded on to a second Ni-NTA agarose column (2.5 × 2 cm) pre-equilibrated with Buffer C and washed with 30 mL of Buffer C + 25 mM imidazole. $^{\Delta N}$CblD lacking a His-tag eluted in the flow through, was concentrated to 5 mL and dialyzed against 0.5 L Reaction Buffer + 4 mM DTT. The monomer was separated from oligomers by size exclusion chromatography (Superdex 200, 100 mL, GE Healthcare) using the Reaction Buffer and stored at −80°C.

Dealkylation of MeCbl by CblC in the presence of CblD

CblC(40 μM) and MeCbl (20 μM) were mixed in the Reaction Buffer ± CblD (40 μM) at 20 °C in the dark. The reaction was initiated by addition of 1 mM GSH, in a total reaction volume of 150 μL. The UV-visible spectrum was recorded every minute for one hour to

monitor the progress of the reaction. To estimate the dealkylation reaction rate, the reaction was quenched by addition of 37.5 μL ice-cold 10% trifluoroacetic acid (TFA) at the desired reaction time points. The proteins were further denatured by heating at 70 °C for 10 min, and separated by centrifugation at 21,000×g at 4 °C for 10 min. The supernatant containing B_{12} was analyzed by HPLC method as described previously[17] , and the concentration of MeCbl was determined. The concentration of MeCbl remaining in the mixture was fitted to the single exponential equation, $[MeCbl] = y_o + a_1 \times e^{-t \times k_{obs}}$. All steps of sample analyses were performed in the dark to avoid photolysis of MeCbl.

Analysis of the CblD•CblC complex using UV-visible spectroscopy

Since light sensitivity of thiolato-cobalamin species was not observed, experiments were performed in ambient light, with the exception of experiments in which MeCbl was used. When the complex was prepared using CblC•cob(II)alamin these two components were pre-mixed for at least 5 min anaerobically, and then mixed at room temperature (23°C) with various concentrations of CblD in aerobic Reaction Buffer containing 500 U of SOD. The final concentrations of CblC, cob(II)alamin, and CblD were 40 μM, 20 μM and 0–40 μM, respectively. When estimating the affinity of the CblD•CblC complex, the absorption spectrum was recorded every minute for 10 min, until there was no further spectral change. To analyze the kinetics of binding, solutions containing CblC (40 μM) and cob(II)alamin (20 μM) were rapidly mixed with CblD (40 μM) and the reaction was monitored at 19 ± 0.2 °C for 200 s at 0.2 s intervals in stopped-flow spectrophotometer. The absorbance at 473 nm ($\Delta\varepsilon_{473}$ nm = 4.1 mM^{-1}•cm^{-1}) was fitted to a double exponential equation $A_{473nm} = y_o + a_1 \times e^{-t \times k_{app1}} + a_2 \times e^{-t \times k_{app2}}$.

When the complex was prepared using $^{\Delta N}$CblD-thiolato-cob(III)alamin, H_2OCbl (100 μM) was mixed with a slight excess of C262S $^{\Delta N}$CblD (120 μM) at room temperature for > 1 h. Unreacted H_2OCbl was removed by centrifugation in a NanoSep filter device (MWCO=10 kDa, PALL). The resulting C262S $^{\Delta N}$CblD- thiolato-cob(III)alamin complex (25 μM) was then incubated with CblC$^{\Delta C}$ (0–40 μM) in the Reaction Buffer at room temperature (23°C) for 5 min till there was no further spectral change. The absorbance change at 425 nm ($\Delta\varepsilon_{425}$ nm = 5.9 mM^{-1}•cm^{-1}) was used to estimate the faction of complex formation.

Analysis of CblD•CblC complex by gel filtration chromatography

CblC$^{\Delta C}$ was mixed with excess cob(II)alamin or MeCbl under anaerobic conditions, and then mixed with aerobic Reaction Buffer ± $^{\Delta N}$CblD in a total volume of 650 μL. The final concentrations of CblC$^{\Delta C}$, B_{12}, and $^{\Delta N}$CblD were 80 μM, 120 μM, and 80 μM, respectively. The mixture was incubated on ice for 10 min and centrifugation at 21,000 ×g at 4 °C for 10 min. The supernatant (500 μL) was loaded on to a Superdex 75 column (30 mL, GE Healthcare) equilibrated with the Reaction Buffer at 4 °C at a flow rate of 0.5 mL/min. The elution profile was recorded at 280 nm. Under these conditions, the elution volumes for $^{\Delta N}$CblD•CblC$^{\Delta C}$, CblC$^{\Delta C}$ and $^{\Delta N}$CblD were 14.1, 16.6, and 17.7 mL, respectively. Free B_{12} eluted after 25 mL. Alternatively, C262S $^{\Delta N}$CblD was incubated with excess H_2OCbl at room temperature for >1h to form C262S $^{\Delta N}$CblD- thiolato-cob(III)alamin complex. Following removal of excess H_2OCbl by centrifugation in a NanpSep centrifugation devices

(MWCO=10 kDa), C262S $^{\Delta N}$CblD- thiolato-cob(III)alamin was mixed with apo-CblC$^{\Delta C}$ in a total volume of 650 μL. The final concentrations of CblC$^{\Delta C}$ and C262S ΔNCblD- thiolato-cob(III)alamin were 60 μM each.

Isothermal titration calorimetry

CblC$^{\Delta C}$ (10–20 μM) was titrated at 20 °C with 29 × 10 μl injections of C262S $^{\Delta N}$CblD-thiolato-cob(III)alamin (100–200 μM) in the Reaction Buffer. The K_D was determined using a single-site binding model and represents the average of four independent experiments.

Interaction of CblD with H_2OCbl

CblD variants (40 μM) were mixed with H_2OCbl (20 μM) in the Reaction Buffer at room temperature (23 °C). The UV-visible spectrum was recorded every minute for 1 h to monitor reaction progress. The change in absorbance at 351 nm (Δε351nm=11.8 $mM^{-1}cm^{-1}$) was fitted to the single exponential equation $\Delta A_{351nm} = y_o + a_1 \times e^{-t \times k_{obs}1}$ .To estimate the affinity of the interaction,-H_2OCbl (20 μM) is incubated with 0–100 μM CblD for 1 h at room temperature. The resulted concentrations of CblD-thiolato-cob(III)alamin are calculated by A 351nm, and the fraction of CblD-thiolato-cob(III)alamin (y) was fitted into the equation $y = \frac{E_0 + L_0 + K_d - \sqrt{(E_0 + L_0 + K_d)^2 - 4 \times E_0 + L_0}}{2 \times L_0}$, where E_0 and L_0 are the total concentration of CblD and H_2OCbl, respectively.

EPR spectroscopy

The concentrations of reagents in the EPR samples were: 375 μM CblC$^{\Delta C}$, 300 μM cob(II)alamin or cob(II)inamide, 500 μM $^{\Delta N}$CblD in Reaction Buffer. The sample containing cob(II)inamide (300 μM) and GSH (4 mM) was prepared in 0.2 M NaOH + 10 % glycerol. All samples were prepared anaerobically. Continuous-wave EPR spectra were collected on a Bruker Elexsys E500 spectrometer using a Super High Q Cavity (Bruker ER 4122SHQE) and Bruker ER4131VT system. A nitrogen-flow cooling system was used. The following experimental conditions were used: modulation frequency, 100 kHz; modulation amplitude, 10 Gauss; microwave power, 2 mW; temperature; 120 K, microwave frequency, 9.45 GHz. Simulations of the EPR spectra were performed by using the EasySpin toolbox run in MATLAB (v. R2015a; Mathworks, Natick, MA)[38] . Simulations included variation of the electron *g*-tensor and electron-nuclear (^{59}Co) hyperfine tensor, with strain parameters introduced for both *g*- and hyperfine tensor components (see Figure S4 and Table S1).

Crystallography, data collection, processing and refinement

For crystallography, a different truncated form of CblD (Δ108) harboring the C262S mutation was created. The primer sequences for creating the truncation were: AGTGAAAGACATGAGTTTGTGATGGCACAATATGTG AATGAATTTCAG (forward) and CACAAACTCATGTCT-TTCACTGGATCCACGCGGAACCA (reverse).

The resulting C262S $^{\Delta N108}$CblD was purified as described above, concentrated and dialyzed overnight in Buffer D (50 mM Tris-HCl, pH 8.0) + 5 mM DTT. The protein was further purified by size exclusion chromatography (Superdex 200, 120 mL, GE Healthcare) in

Buffer D. The fractions corresponding to monomeric C262S $^{\Delta N}$CblD were pooled, concentrated and incubated overnight at 4°C with H_2OCbl (1.5 equivalents) to form the C262S $^{\Delta N}$CblD -thiolato-cob(III)alamin complex. Unreacted H_2OCbl was separated from C262S $^{\Delta N}$CblD -thiolato-cob(III)almin by size exclusion chromatography in Buffer D (Superdex 200, 120 mL, GE Healthcare).

C262S $^{\Delta N}$CblD -thiolato-cob(III)alamin in Buffer D + 0.5 mM Tris (2-carboxyethyl) phosphine (TCEP) was used for screening crystallization conditions. Crystals appeared in well solution containing 20% PEG 8000, 100 mM Tris-HCl, pH 8.5, and 200 mM $MgCl_2$ incubated at 20°C. Crystals with the best morphology were obtained by the hanging drop vapor diffusion method from a 2:1 mixture of protein (20 mg•mL^{-1}) to well solution in 2–4 μL drops. For data collection, crystals were soaked in a cryoprotectant solution (well solution, 20% v/v glycerol) and flash cooled in liquid nitrogen.

Data sets were collected at the LS-CAT (21-G), Argonne National Laboratory (ANL). Diffraction data were collected at a wavelength of 0.98 Å and 100 °K using a MARMOSAIC 300 mm Charge Coupled Device (CCD) detector. The data were indexed and integrated using DIALS[39] and scaled in Aimless[40] to a resolution of 2.5 Å. Data collection statistics are summarized in Table S3. The structure of C262S $^{\Delta N}$CblD -thiolato-cob(III)alamin was solved by molecular replacement using Phaser[41] in the CCP4 program suit[40] . The initial search model was the previously published structure of apo-CblD (PDB code: 5CV0)[19]. Crystals of C262S $^{\Delta N}$CblD -thiolato-cob(III)alamin were of the space group C 1 2 1 (103.2, 69.8, 64.3, 90, 101, 90) with two chains per asymmetric unit. Iterative rounds of model building and refinement were performed with COOT[42] and Phenix[43]. Ligand restraints were generated in eLBOW[44]. The Co-S bond length and S-Co-N angles were restrained during refinement using the parameters from EXAFS and the crystal structure of GSCbl[45]. Final refinement statistics are presented in Table S3. Ramachandran statistics are favored (96%), allowed (4%) and outliers (0%). The geometric quality of the model was assessed in MolProbity[46] with a final score of 1.26 and 100th percentile. Structural figures were made using UCSF Chimera[47].

XAS Spectroscopy

The samples were prepared in buffer containing 100 mM HEPES-KOH, pH 7.4, and 30% glycerol. GSCbl was prepared by incubating H_2OCbl with excess of GSH. C262S $^{\Delta N}$CblD -thiolato-cob(III)alamin was prepared by incubating H_2OCbl (0.8 mM) with 1.2 equivalents of C262S $^{\Delta N}$CblD. Excess CblC$^{\Delta C}$ (1.5 equivalents) was then added to C262S $^{\Delta N}$CblD -thiolato-cob(III)alamin in the presence or absence of 1 mM GSMe. Formation of thiolato-cob(III)alamin was confirmed by the absorption spectrum and were flash frozen in liquid nitrogen. XAS data were collected at the Stanford Synchrotron Radiation Lightsource (SSRL) beamline 9–3. The beamline is equipped with a Si (220) double crystal monochromator and a flat Rh-coated harmonic rejection mirror. The samples were maintained at ~10 K in an Oxford Instruments liquid helium cryostat. The data were collected in the fluorescence mode utilizing a 100 element Ge-detector equipped with an Fe filter and Soller slits focused on the sample. The data were normalized to the incident intensity which was measured with a N_2 filled ion chamber. The spectra were collected

using 10 eV steps and 1 second integration times in the pre-edge region, 0.25 eV steps/1 second in the edge region, and 0.05 $Å^{-1}$ steps in the EXAFS region with k^3-weighted integration times running from 1 to 20 s, for a total measurement time of ~40 min per scan. The X-ray energies were calibrated by simultaneously measuring the absorption spectrum of a cobalt foil, with the first inflection point assigned as 7709 eV. EXAFS data were analyzed using EXAFSPAK (https://www-ssrl.slac.stanford.edu/~george/exafspak/exafs.htm) and FEFF 9.0[48] . XANES data were normalized using MBACK[49].

Fits of the EXAFS data used the most important single and double-scattering pathways out to 3.4 Å (see Table S2 for more details). A number of cobalamin distortions were considered as possible explanations for the observed differences (EXAFS amplitude at ~ k = 6–8 $Å^{-1}$; Fourier transform peak position at ~2.3 Å). No distortion in the corrin structure and no change in Co-N/O coordination number reproduced these changes. In order to reproduce these changes, it was necessary to include a shell of sulfur at ~2.3 Å in the base-on samples. Although a sulfur ligand is expected, based on the UV-visible spectra (Figure 4a,b), inclusion of this shell gave only a modest improvement in fit quality and it would be difficult to establish the presence of this shell using EXAFS alone.

Inclusion of a Co-S shell in fits to the base-off samples gave only a marginal improvement in the fit, and the Co-S distance refined either to a chemically unreasonable distance (~2.05–2.15 Å) or to a much longer distance (~2.57 Å). The latter is long for EXAFS detection, and, not surprisingly, this interaction has a high Debye-Waller factor. It would not be possible to establish unequivocally from EXAFS alone that this shell makes a significant contribution to the EXAFS; however, given the spectral evidence (Figure 1g) for a Co-thiolato interaction, we favor this as our best estimate for the Co-S distance in the base-off samples. The difference between “normal” Co-S distances for base-on and “long” Co-S distances for base-off is sufficient to explain the differences in the EXAFS (see Figure S7).

Supplementary Material

Refer to Web version on PubMed Central for supplementary material.

ACKNOWLEDGMENT

We acknowledge the LS-CAT beamline 21-ID-G at the Advanced Proton Source (Argonne National Labs) for X-ray beam time. Use of the Stanford Synchrotron Radiation Lightsource, SLAC National Accelerator Laboratory, was supported by the DOE (DEAC02-76SF00515). The SSRL Structural Molecular Biology Program was supported by the DOE Office of Biological and Environmental Research and by NIGMS (P41GM103393).

Funding Sources

This work was supported in part by grants from the National Institutes of Health (R01-DK045776 to RB, R01-DK054514 to KW), the American Heart Association (19POST34370113 to RM) and from the National Science Foundation (NSF-CHE 1945174 to MK).

ABBREVIATIONS

Cob(II)	cob(II)alamin
Cbi(II)	cob(II)inamide

MeCbl	methylcobalamin
DMB	dimethylbenzimidazole
GSCbl	glutathionylcobalamin
H_2OCbl	aquocobalamin
GSH	glutathione
GSMe	S-methylglutathione
EPR	electron paramagnetic spectroscopy
XAS	X-ray absorption spectroscopy
XANES	X-ray absorption near edge spectroscopy
EXAFS	extended X-ray absorption fine structure

REFERENCES

1. Banerjee R; Ragsdale SW, The Many Faces of Vitamin B12: Catalysis by Cobalamin-Dependent Enzymes. Ann. Rev. Biochem 2003, 72, 209–247. [PubMed: 14527323]
2. Banerjee R, B12 Trafficking in Mammals: A Case for Coenzyme Escort Service. ACS Chem. Biol 2006, 1 (3), 149–59. [PubMed: 17163662]
3. Banerjee R; Gherasim C; Padovani D, The Tinker, Tailor, Soldier in Intracellular B12 Trafficking. Cur. Op. Chem. Biol 2009, 13, 484–91.
4. Gherasim C; Lofgren M; Banerjee R, Navigating the B_{12} Road: Assimilation, Delivery and Disorders of Cobalamin. J. Biol. Chem 2013, 288, 13186–93. [PubMed: 23539619]
5. Watkins D; Rosenblatt DS, Inborn Errors of Cobalamin Absorption and Metabolism. Am. J. Med. Genet. C Semin. Med. Genet 2011, 157C (1), 33–44. [PubMed: 21312325]
6. Lerner-Ellis JP; Tirone JC; Pawelek PD; Dore C; Atkinson JL; Watkins D; Morel CF; Fujiwara TM; Moras E; Hosack AR; Dunbar GV; Antonicka H; Forgetta V; Dobson CM; Leclerc D; Gravel RA; Shoubridge EA; Coulton JW; Lepage P; Rommens JM; Morgan K; Rosenblatt DS, Identification of the Gene Responsible for Methylmalonic Aciduria and Homocystinuria, *cblC* Type. Nat. Genet 2006, 38 (1), 93–100. [PubMed: 16311595]
7. Kim J; Hannibal L; Gherasim C; Jacobsen DW; Banerjee R, A Human Vitamin B_{12} Trafficking Protein Uses Glutathione Transferase Activity for Processing Alkylcobalamins. J. Biol. Chem 2009, 284 (48), 33418–24. [PubMed: 19801555]
8. Kim J; Gherasim C; Banerjee R, Decyanation of Vitamin B_{12} by a Trafficking Chaperone. Proc. Natl. Acad. Sci. U.S.A 2008, 105 (38), 14551–4. [PubMed: 18779575]
9. Li Z; Gherasim C; Lesniak NA; Banerjee R, Glutathione-Dependent One-Electron Transfer Reactions Catalyzed by a B_{12} Trafficking Protein. J. Biol. Chem 2014, 289 (23), 16487–16497. [PubMed: 24742678]
10. Froese DS; Healy S; McDonald M; Kochan G; Oppermann U; Niesen FH; Gravel RA, Thermolability of Mutant MMACHC Protein in the Vitamin B12-Responsive *cblC Disorder*. Mol. Genet. Metab 2010, 100 (1), 29–36. [PubMed: 20219402]
11. Froese DS; Krojer T; Wu X; Shrestha R; Kiyani W; von Delft F; Gravel RA; Oppermann U; Yue WW, Structure of MMACHC Reveals an Arginine-Rich Pocket and a Domain-Swapped Dimer for Its B12 Processing Function. Biochemistry-Us 2012, 51 (25), 5083–90.
12. Gherasim C; Ruetz M; Li Z; Hudolin S; Banerjee R, Pathogenic Mutations Differentially Affect the Catalytic Activities of the Human B_{12}-Processing Chaperone CblC and Increase Futile Redox Cycling. J. Biol. Chem 2015, 290 (18), 11393–402. [PubMed: 25809485]

13. Hannibal L; Kim J; Brasch NE; Wang S; Rosenblatt DS; Banerjee R; Jacobsen DW, Processing of Alkylcobalamins in Mammalian Cells: A Role for the MMACHC (cblC) Gene Product. Mol. Genet. Metab 2009, 97 (4), 260–6. [PubMed: 19447654]

14. Jeong J; Kim J, Glutathione Increases the Binding Affinity of a Bovine B_{12} Trafficking Chaperone bCblC for Vitamin B_{12}. Biochem. Biophys. Res. Commun 2011, 412 (2), 360–5. [PubMed: 21821010]

15. Jeong J; Park J; Kim J, Processing of Glutathionylcobalamin by a Bovine B_{12} Trafficking Chaperone bCblC Involved in Intracellular B_{12} Metabolism. Biochem. Biophys. Res. Commun 2014, 443 (1), 173–8. [PubMed: 24286755]

16. Koutmos M; Gherasim C; Smith JL; Banerjee R, Structural Basis of Multifunctionality in a Vitamin B_{12}-Processing Enzyme. J. Biol. Chem 2011, 286 (34), 29780–7. [PubMed: 21697092]

17. Li Z; Lesniak NA; Banerjee R, Unusual Aerobic Stabilization of Cob(I)Alamin by a B12-Trafficking Protein Allows Chemoenzymatic Synthesis of Organocobalamins. J. Am. Chem. Soc 2014, 136 (46), 16108–11. [PubMed: 25369151]

18. Ruetz M; Shanmuganathan A; Gherasim C; Karasik A; Salchner R; Kieninger C; Wurst K; Banerjee R; Koutmos M; Krautler B, Antivitamin B-12 Inhibition of the Human B-12-Processing Enzyme CblC: Crystal Structure of an Inactive Ternary Complex with Glutathione as the Cosubstrate. Angew. Chem. Int. Edit 2017, 56 (26), 7387–7392.

19. Yamada K; Gherasim C; Banerjee R; Koutmos M, Structure of Human B-12 Trafficking Protein CblD Reveals Molecular Mimicry and Identifies a New Subfamily of Nitro-FMN Reductases. . J. Biol. Chem 2015, 290 (49), 29155–29166. [PubMed: 26364851]

20. Froese DS; Kopec J; Fitzpatrick F; Schuller M; McCorvie TJ; Chalk R; Plessl T; Fettelschoss V; Fowler B; Baumgartner MR; Yue WW, Structural Insights into the MMACHC-MMADHC Protein Complex Involved in Vitamin B-12 Trafficking. . J. Biol. Chem 2015, 290 (49), 29167–29177. [PubMed: 26483544]

21. Deme JC; Miousse IR; Plesa M; Kim JC; Hancock MA; Mah W; Rosenblatt DS; Coulton JW, Structural Features of Recombinant MMADHC Isoforms and Their Interactions with Mmachc, Proteins of Mammalian Vitamin B12 Metabolism. Mol. Genet. Metab 2012, 107 (3), 352–62. [PubMed: 22832074]

22. Gherasim C; Hannibal L; Rajagopalan D; Jacobsen DW; Banerjee R, The C-Terminal Domain of CblD Interacts with CblC and Influences Intracellular Cobalamin Partitioning. Biochimie 2013, 95 (5), 1023–32. [PubMed: 23415655]

23. Plesa M; Kim J; Paquette SG; Gagnon H; Ng-Thow-Hing C; Gibbs BF; Hancock MA; Rosenblatt DS; Coulton JW, Interaction between MMACHC and MMADHC, Two Human Proteins Participating in Intracellular Vitamin B-12 Metabolism. Mol. Genet. Metab 2011, 102 (2), 139–148. [PubMed: 21071249]

24. Li Z; Shanmuganathan A; Ruetz M; Yamada K; Lesniak NA; Krautler B; Brunold TC; Koutmos M; Banerjee R, Coordination Chemistry Controls the Thiol Oxidase Activity of the B_{-12}-Trafficking Protein CblC. J. Biol. Chem 2017, 292 (23), 9733–9744. [PubMed: 28442570]

25. Lexa D; Saveant J-M, The Electrochemistry of Vitamin B12. Acc. Chem. Res 1983, 16, 235–243.

26. Muir Wood P, The Redox Potential of the System Oxygen--Superoxide. FEBS Lett. 1974, 44 (1), 22–4. [PubMed: 4855030]

27. Krautler B, Thermodynamic Trans-Effects of the Nucleotide Base in the B-12 Coenzymes. Helv. Chim. Acta 1987, 70 (5), 1268–1278.

28. Stich TA; Buan NR; Brunold TC, Spectroscopic and Computational Studies of Co^{2+} Corrinoids: Spectral and Electronic Properties of the Biologically Relevant Base-on and Base-Off Forms of Co^{2+} Cobalamin. J. Am. Chem. Soc 2004, 126 (31), 9735–9749. [PubMed: 15291577]

29. Suarez-Moreira E; Hannibal L; Smith CA; Chavez RA; Jacobsen DW; Brasch NE, A Simple, Convenient Method to Synthesize Cobalamins: Synthesis of Homocysteinylcobalamin, N-Acetylcysteinylcobalamin, 2-N-Acetylamino-2-Carbomethoxyethanethiolatocobalamin, Sulfitocobalamin and Nitrocobalamin. Dalton Transactions 2006, (44), 5269–77. [PubMed: 17088966]

30. Schrapers P; Mebs S; Goetzl S; Hennig SE; Dau H; Dobbek H; Haumann M, Axial Ligation and Redox Changes at the Cobalt Ion in Cobalamin Bound to Corrinoid Iron-Sulfur Protein (CoFeSP) or in Solution Characterized by XAS and DFT. Plos One 2016, 11 (7).

31. Camponeschi F; Banci L, Metal Cofactors Trafficking and Assembly in the Cell: A Molecular View. Pure Appl. Chem 2019, 91 (2), 231–245.

32. Reddi AR; Hamza I, Heme Mobilization in Animals: A Metallolipid's Journey. Accounts Chem. Res 2016, 49 (6), 1104–1110.

33. Parks JM; Johs A; Podar M; Bridou R; Hurt RA; Smith SD; Tomanicek SJ; Qian Y; Brown SD; Brandt CC; Palumbo AV; Smith JC; Wall JD; Elias DA; Liang LY, The Genetic Basis for Bacterial Mercury Methylation. Science 2013, 339 (6125), 1332–1335. [PubMed: 23393089]

34. Rempel S; Colucci E; de Gier JW; Guskov A; Slot-boom DJ, Cysteine-Mediated Decyanation of Vitamin B12 by the Predicted Membrane Transporter BtuM. Nat. Commun 2018, 9, 3038. [PubMed: 30072686]

35. Coelho D; Suormala T; Stucki M; Lerner-Ellis JP; Rosenblatt DS; Newbold RF; Baumgartner MR; Fowler B, Gene Identification for the *cblD* Defect of Vitamin B-12 Metabolism. New Engl. J. Med 2008, 358 (14), 1454–1464. [PubMed: 18385497]

36. Li Z; Kitanishi K; Twahir UT; Cracan V; Chapman D; Warncke K; Banerjee R, Cofactor Editing by the G-Protein Metallochaperone Domain Regulates the Radical B_{12} Enzyme IcmF. . J. Biol. Chem 2017, 292 (10), 3977–3987. [PubMed: 28130442]

37. Ishida A; Ichikawa M; Kobayashi K; Hitomi T; Kojima S; Toraya T, Importance of the Nucleotide Loop Moiety Coordinated to the Cobalt Atom of Adenosylcobalamin for Coenzymic Function in the Diol Dehydrase Reaction. J. Nutr. Sci. Vitaminol. (Tokyo) 1993, 39 (2), 115–25. [PubMed: 8410372]

38. Stoll S; Schweiger A, Easyspin, a Comprehensive Software Package for Spectral Simulation and Analysis in EPR. J. Magn. Reson 2006, 178 (1), 42–55. [PubMed: 16188474]

39. Clabbers MTB; Gruene T; Parkhurst JM; Abrahams JP; Waterman DG, Electron Diffraction Data Processing with DIALS. Acta Crystallogr. D Struct. Biol 2018, 74, 506–518. [PubMed: 29872002]

40. Winn MD; Ballard CC; Cowtan KD; Dodson EJ; Emsley P; Evans PR; Keegan RM; Krissinel EB; Leslie AGW; McCoy A; McNicholas SJ; Murshudov GN; Pannu NS; Potterton EA; Powell HR; Read RJ; Vagin A; Wilson KS, Overview of the CCP4 Suite and Current Developments. Acta Crystallogr. D 2011, 67, 235–242. [PubMed: 21460441]

41. McCoy AJ; Grosse-Kunstleve RW; Adams PD; Winn MD; Storoni LC; Read RJ, Phaser Crystallographic Software. J. Appl. Crystallogr 2007, 40 (Pt 4), 658–674. [PubMed: 19461840]

42. Emsley P; Lohkamp B; Scott WG; Cowtan K, Features and Development of Coot. Acta Crystallogr. D Biol. Crystallogr 2010, 66 (Pt 4), 486–501. [PubMed: 20383002]

43. Afonine PV; Grosse-Kunstleve RW; Echols N; Headd JJ; Moriarty NW; Mustyakimov M; Terwilliger TC; Urzhumtsev A; Zwart PH; Adams PD, Towards Automated Crystallographic Structure Refinement with Phenix.Refine. Acta Crystallogr. D Biol. Crystallogr 2012, 68 (Pt 4), 352–67. [PubMed: 22505256]

44. Moriarty NW; Grosse-Kunstleve RW; Adams PD, Electronic Ligand Builder and Optimization Workbench (eLBOW): A Tool for Ligand Coordinate and Restraint Generation. Acta Crystallogr. D Biol. Crystallogr 2009, 65 (Pt 10), 1074–80. [PubMed: 19770504]

45. Hannibal L; Smith CA; Jacobsen DW, The X-Ray Crystal Structure of Glutathionylcobalamin Revealed. Inorg. Chem 2010, 49 (21), 9921–9927. [PubMed: 20863098]

46. Williams CJ; Headd JJ; Moriarty NW; Prisant MG; Videau LL; Deis LN; Verma V; Keedy DA; Hintze BJ; Chen VB; Jain S; Lewis SM; Arendall WB 3rd; Snoeyink J; Adams PD; Lovell SC; Richardson JS; Richardson DC, MolProbity: More and Better Reference Data for Improved All-Atom Structure Validation. Protein Sci. 2018, 27 (1), 293–315. [PubMed: 29067766]

47. Pettersen EF; Goddard TD; Huang CC; Couch GS; Greenblatt DM; Meng EC; Ferrin TE, UCSF Chimera--a Visualization System for Exploratory Research and Analysis. J. Comput. Chem 2004, 25 (13), 1605–12. [PubMed: 15264254]

48. Ankudinov AL; Rehr JJ, Relativistic Calculations of Spin-Dependent X-Ray-Absorption Spectra. Phys. Rev. B 1997, 56 (4), R1712–R1716.

49. Weng TC; Waldo GS; Penner-Hahn JE, A Method for Normalization of X-Ray Absorption Spectra. J. Synchrotron. Radiat 2005, 12 (Pt 4), 506–10. [PubMed: 15968130]

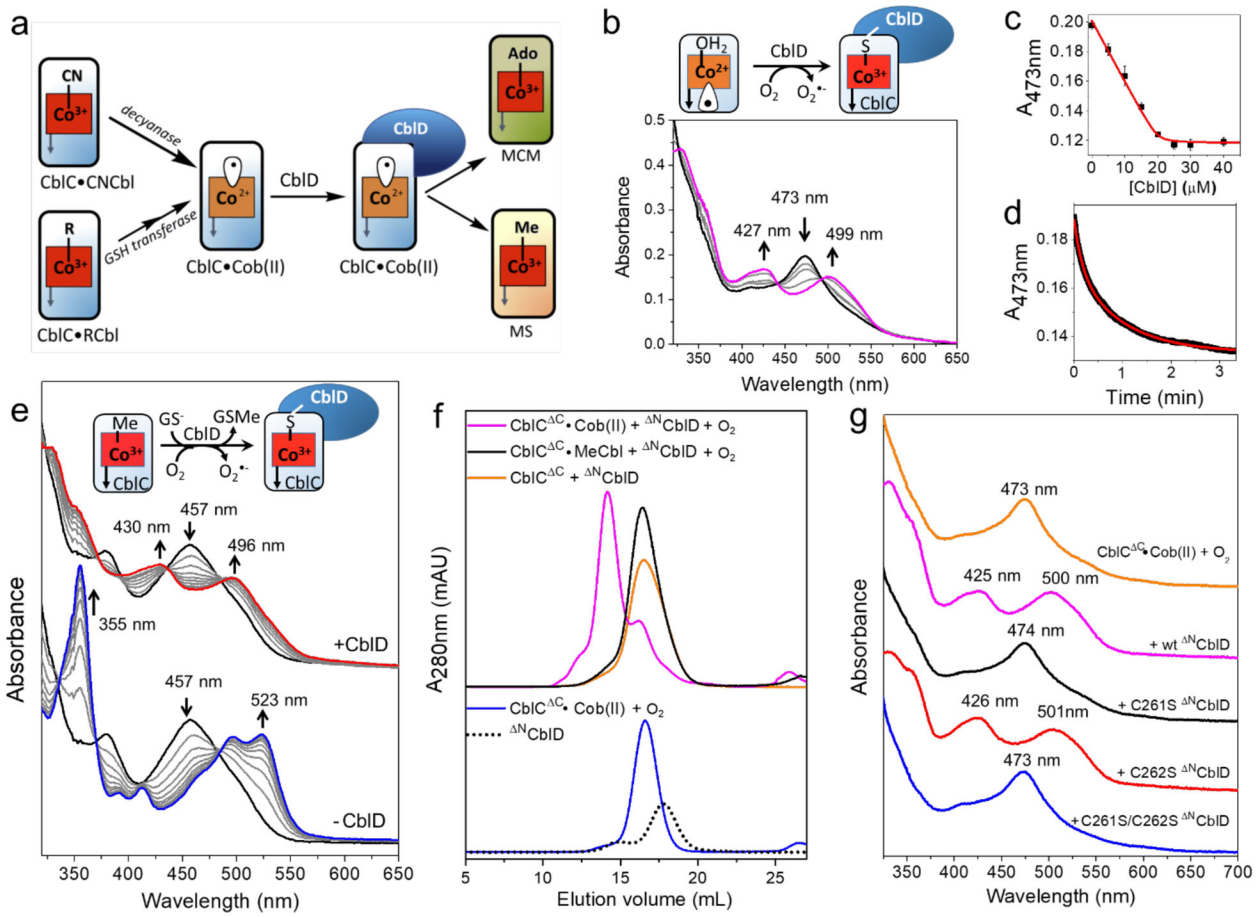

FIGURE 1.

CblD forms a complex with CblC•cob(II)alamin in the presence of O_2. (a) Roles of CblC and CblD in processing and downstream partitioning B_{12}. MS, MCM and RCbl denote methionine synthase, methylmalonyl-CoA synthase and alkylcobalamin, respectively. The base-off state of B_{12} is denoted by the straight arrow connected to the corrin ring. (b, c) UV-visible spectra of the CblD•CblC complex. Changes in the absorption spectrum of CblC (40 μM)-bound cob(II)alamin (20 μM) (*black*) following mixing with CblD (0–25 μM) under aerobic conditions. SOD (>500 U) was added to prevent $O_2^{\bullet-}$ accumulation. The gray and magenta lines represent intermediate and final spectra, respectively. The dependence of A473 nm on CblD concentration is shown in (c). (d) Kinetics of CblD•CblC complex formation. CblC (30 μM) and cob(II)alamin (15 μM) were mixed with CblD (30 μM) and SOD (>500 U) under aerobic conditions. The time-dependent changes in A473 nm (*black*) were fitted (*red*) to a double exponential equation. (e) Spectral changes during the aerobic dealkylation of CblC•MeCbl in the presence of CblD. *Upper.* To CblC (40 μM)-bound MeCbl (20 μM), CblD (40 μM) and GSH (1 mM) were added. The black and red lines represent the initial and final (60 min) spectra. *Lower.* To CblC (40 μM)-bound MeCbl (20 μM), GSH (1 mM) was added. The black and blue lines represent the initial and final (60 min) spectra, respectively. (f) Size exclusion chromatography of the $^{\Delta N}$CblD•CblC$^{\Delta C}$ complex. *Upper.* Elution profiles of aerobic samples as labeled in the figure containing CblC$^{\Delta C}$ and/or $^{\Delta N}$CblD (80 μM each) and B_{12} (120 μM). (g) UV-visible analysis of complex

formation. The samples as labeled in the figure contained: $CblC^{\Delta C}$ (40 μM), cob(II)alamin (20 μM) and $^{\Delta N}CblD$ (40 μM) and were incubated aerobically for 5 min.

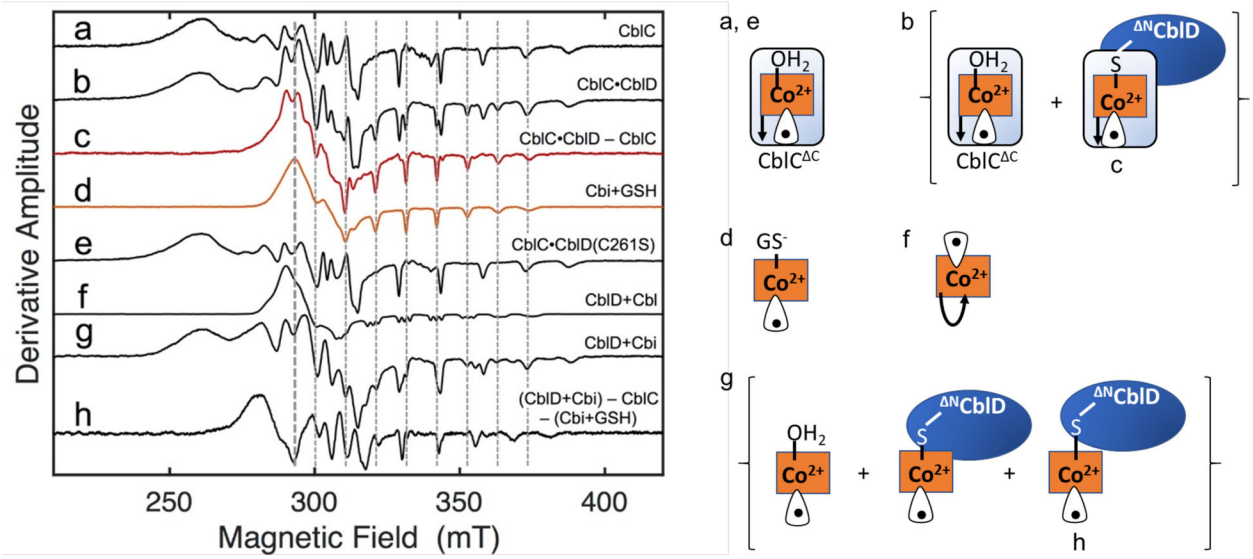

FIGURE 2.

EPR spectroscopy reveals the presence of a thiolato-cob(II)alamin species in the CblD•CblC complex. The experiments were performed in the absence of O_2. (a-c) Characterization of Co-S ligation by comparison of the EPR spectra of $CblC^{\Delta C}$•cob(II)alamin alone (a), or mixed with wild-type $^{\Delta N}$CblD (b), or following deconvolution (c), by subtraction of scaled (a). (d) The spectrum of cob(II)inamide mixed with glutathione (GSH) under alkaline conditions revealed positions of the signature Co hyperfine octet features that are split symmetrically about the high-field g_z position (vertical dashed lines), and low-field peak feature (thick vertical dashed line) characteristic of an axial *g*-tensor. (e) The high-field octet splitting due to Co-S ligation is not seen when C261S $^{\Delta N}$CblD is added to $CblC^{\Delta C}$•cob(II)alamin. (f,g) $^{\Delta N}$CblD does not coordinate cob(II)alamin (f) but interacts via Co-S ligation with cob(II)inamide (g). (h) Spectral deconvolution of (g), by subtraction of scaled (a) and (d), reveals the presence of a third species, which appears to interact with CblD. The concentrations of $CblC^{\Delta C}$, $^{\Delta N}$CblD, cobalamin, cobinamide and GSH were 375 μM, 500 μM, 300 μM, 300 μM and 4 mM, respectively. Free electron $g = 2.002$ corresponds to 337.1 mT. The curved versus straight arrows under the corrin ring denote the base-on versus base-off coordination states.

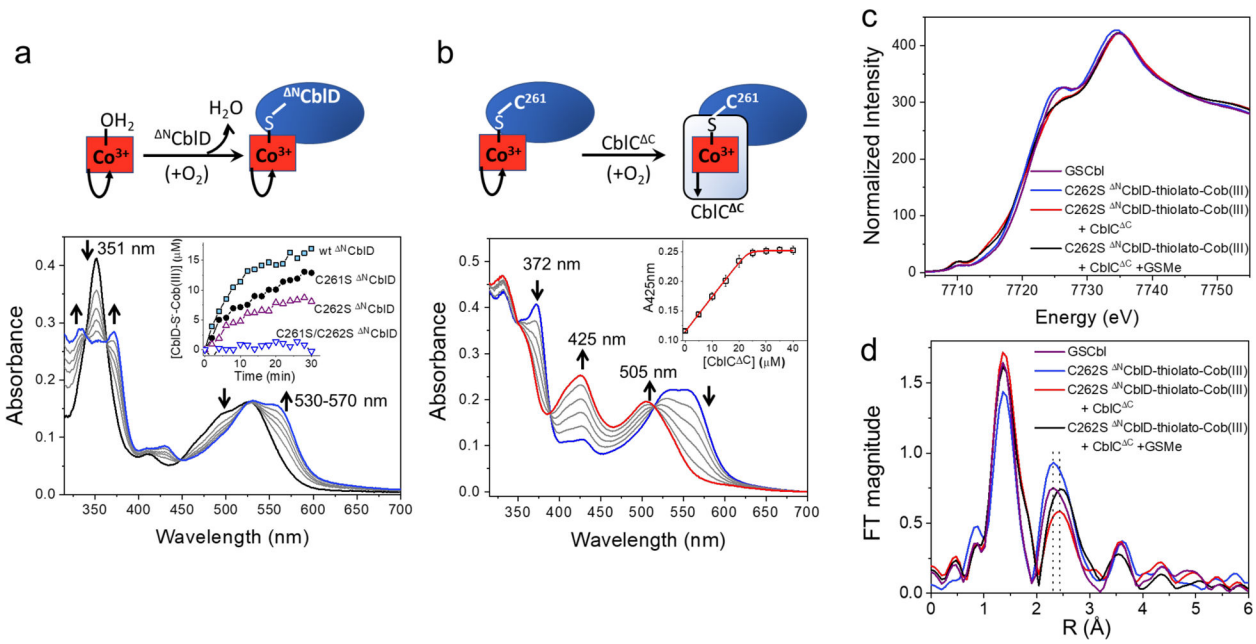

FIGURE 3.

$^{\Delta N}$CblD binds H_2OCbl. (a) Spectral changes induced by H_2OCbl (20 μM) binding to $^{\Delta N}$CblD (40 μM). The initial and final (60 min) spectra are in black and blue, respectively. *Inset.* Time-dependent changes in CblD-thiolato-cob(III)alamin concentration upon aerobic incubation of H_2OCbl (40 μM) with wild-type, C261S or C262S $^{\Delta N}$CblD (40 μM each) as indicated. (b) Spectral changes upon mixing C262S $^{\Delta N}$CblD-thiolato-cob(III)alamin (25 μM) with CblC$^{\Delta C}$ (0–40 μM), reflecting the base-on to base-off conversion of thiolato-cob(III)alamin induced by formation of the $^{\Delta N}$CblD•CblC$^{\Delta C}$ complex. The initial spectrum of C262S $^{\Delta N}$CblD-thiolato-cob(III)alamin is in blue and the final spectrum of the C262S $^{\Delta N}$CblD-thiolato-cob(III)alamin•CblC$^{\Delta C}$ complex is in red. *Inset.* Dependence of A425 nm on the concentration of CblC$^{\Delta C}$. (c, d) Normalized XANES (c) and EXAFS (d) spectra of thiolato-cob(III)alamin species under aerobic conditions. Base-on GSCbl (*purple*), C262S $^{\Delta N}$CblD-thiolato-cob(III)alamin (*blue*). C262S $^{\Delta N}$CblD-thiolato-cob(III)alamin•CblC$^{\Delta C}$ (*red*) and C262S $^{\Delta N}$CblD-thiolato-cob(III)alamin•CblC$^{\Delta C}$ +GSMe (*black*). Dotted lines at R=2.31 and 2.44 Å mark the maxima in the peaks for the base-on and base-off samples, respectively. The curved versus straight arrow under the corrin ring denotes the base-on versus base-off states of cobalamin, respectively.

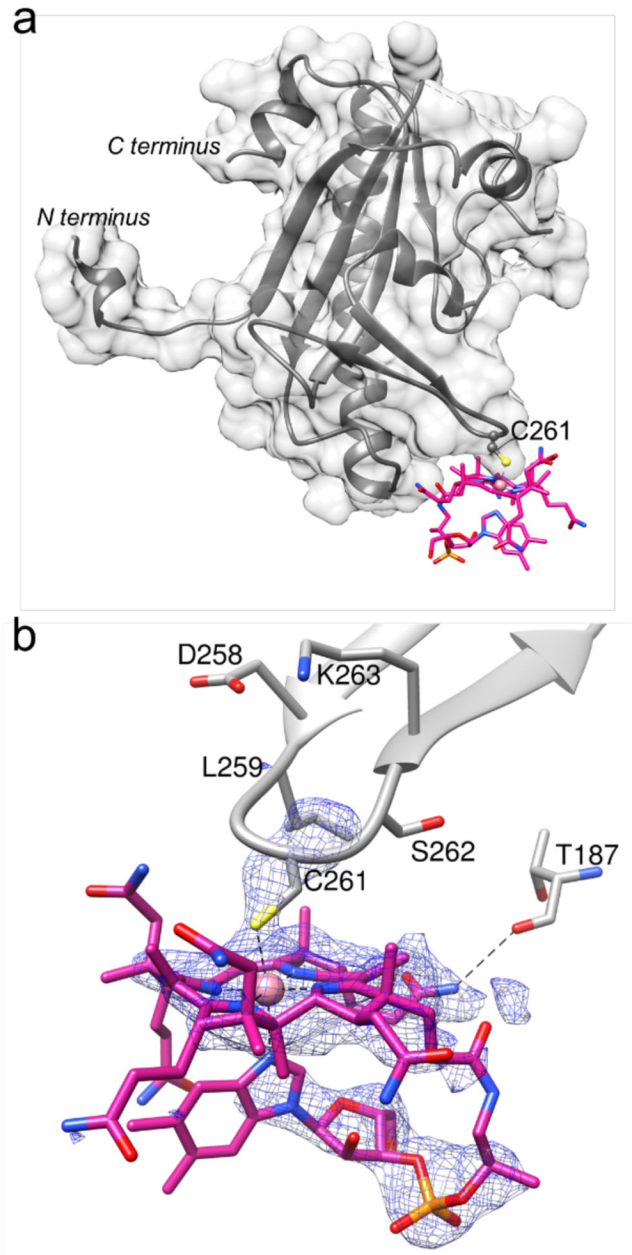

FIGURE 4.

Structure of CblD reveals thiolato-cob(III)alamin. (a) Surface and ribbon representation of C262S $^{\Delta N108}$CblD (*grey*) bound to cobalamin (*violet* stick display) via a Co-S bond formed between Cys-261 and the cobalt ion. (b) A close-up showing the interactions between cobalamin and CblD with superimposition of the Fo-Fc simulated annealing omit map of cobalamin and Cys-261 at 2.5 σ.

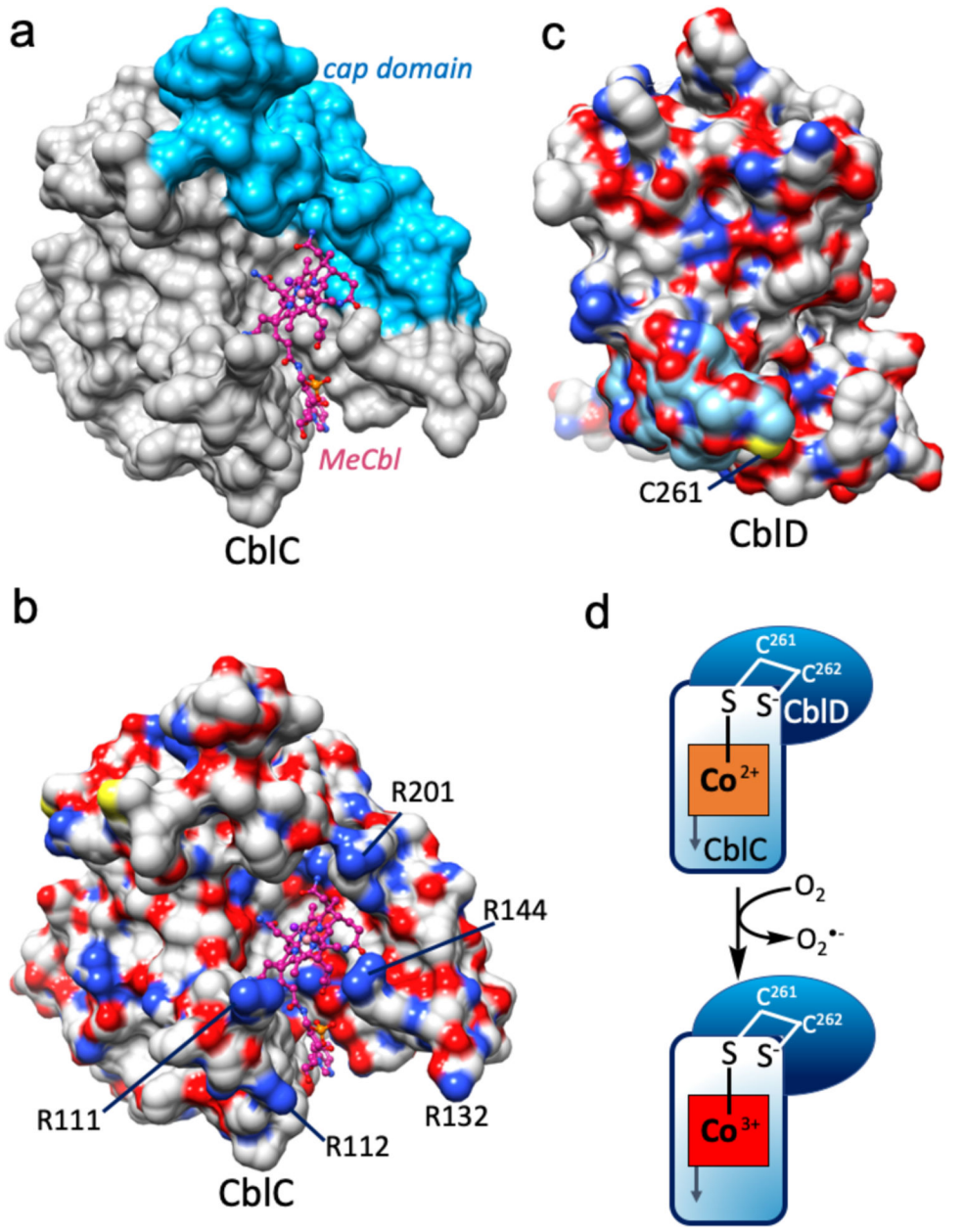

FIGURES 5.

Summary of metal-mediated interactions between CblC and CblD. (a) Surface representation of the human CblC structure with MeCbl (*magenta*) bound (PDB ID:3SC0). The cap domain is shown in blue. (b) Electrostatic surface potential of CblC shows that the entrance to the active site is highly electropositive. (c) Electrostatic surface potential of human CblD (PDB ID: 5CV0) shows a mix of electropositive and electronegative patches. The β-hairpin (*light blue*) bearing Cys-261 which coordinates the cobalt ion, is largely electroneutral with a few electronegative residues. (d) Scheme showing mechanism of CblD•CblC complex is initiated in the cob(II)alamin state that is subsequently oxidized.

CblD + CblC•**Cob(II)** + O_2 → CblD-**thiolato-Cob(III)**•CblC + $O_2^{\bullet-}$ (reaction 1)

CblD + CblC•**MeCbl** + GS^- + $2O_2$ → CblD-**thiolato-Cob(III)**•CblC + GSMe + $2O_2^{\bullet-}$ (reaction 2)

CblC•**MeCbl** + GS^- → CblC•**cob(I)alamin** + GSMe (reaction 3)

CblC•**cob(I)alamin** + O_2 → CblC•**cob(II)alamin** + $O_2^{\bullet-}$ (reaction 4)

CblD-S^- + CblC•**cob(II)alamin** ↔ CblD-**thiolato-cob(II)alamin**•CblC (reaction 5)

CblD-**thiolato-Cob(II)**•CblC + O_2 → CblD-**thiolato-Cob(III)**•CblC + $O_2^{\bullet-}$ (reaction 6)

CblC•**MeCbl** + GSH + O_2 + H_2O + H^+ → CblC•**H_2OCbl** + GSMe + H_2O_2 (reaction 7)

CblD-S^- + CblC•**H_2OCbl** → CblD-**thiolato-cob(III)alamin**•CblC + H_2O (reaction 8)

CblD-S^- + **H_2OCbl** → CblD-**thiolato-Cob(III)** + H_2O (reaction 9)

SCHEME 1.

Reactions catalyzed by CblC and cobalamin coordination complexes with CblC and CblD.